Diffusion-Controlled Photochemical Reactions in Membranes. Photodimerization of 6-(9-Anthroyloxy) Stearic Acid in POPC Bilayers under Steady-State Irradiation

ARTICLE · NOVEMBER 1999

DOI: 10.1021/jp9918196

2 AUTHORS:

Maria João Moreno
University of Coimbra
47 PUBLICATIONS **545** CITATIONS
SEE PROFILE

Eurico Melo
New University of Lisbon
57 PUBLICATIONS **1,085** CITATIONS
SEE PROFILE

Diffusion-Controlled Photochemical Reactions in Membranes. Photodimerization of 6-(9-Anthroyloxy) Stearic Acid in POPC Bilayers under Steady-State Irradiation

Maria João Moreno[†] and Eurico Melo*[,†,‡]

Instituto de Tecnologia Química e Biológica, Oeiras, Portugal, and Instituto Superior Técnico, Lisboa, Portugal

Received: June 3, 1999; In Final Form: August 24, 1999

We present a detailed study of the models for diffusion controlled bimolecular reactions in phospholipid membranes analyzing the case of the photodimerization of long lived (200 ns) and short lived (10 ns) excited species under steady state irradiation. It is shown that only when using the 2D formalism for the diffusion-controlled rate constant, k_{diff}, do the parameters retrieved have physical meaning. In certain cases the use of a 3D law instead of the 2D specific law does not lead to significantly different results. However, this agreement between the two models is misleading and depends on the specific system, namely on the way the 3D concentration is calculated and on the position of the reactant relative to the center of the bilayer. The models were tested for the photodimerization of 6-(9-anthroyloxy)stearic acid (6-AS) in a membrane model system of 1-palmitoyl-2-oleoyl-*sn*-glycero-3-phosphocholine (POPC). The quenching of the excited state is diffusion controlled but only a fraction of quenching, γ, leads to dimerization. Since we know from independent measurements that γ must vary between 0.05 and 0.1 we may conclude that the value of $\gamma = 0.3$ obtained with the 3D law without considering the time dependence of k_{diff} is out of range, while $\gamma \approx 0.1$ obtained for both 2D and 3D complete laws is acceptable. We further discuss the physical meaning of the application of the 3D law to this system and the method used for the calculation of the 3D concentration. The lateral diffusion coefficient of the reactants, necessary for the calculations, was independently measured in a model system using the technique of fluorescence recovery after photobleaching.

Introduction

Bimolecular reactions that take place in phospholipid bilayers are the key of many biochemical processes. The kinetics of diffusion-controlled and near diffusion-controlled reactions in biological membranes is characterized by the properties of the reaction media, namely the two-dimensional geometry and the high viscosity. If the membrane space is heterogeneous in such a way that the reagents become isolated in small domains, the kinetics and yield are also affected by the distribution of reagents by the compartments of the membrane.[1] Despite its importance, bimolecular reactions in simple model systems such as synthetic bilayers have not yet been the subject of much attention and we are far from a complete awareness of the effect of each of the mentioned membrane properties in the reaction kinetics and yield. In the present work we will address the relationship between bimolecular kinetics and molecular parameters in a homogeneous bilayer.

An appropriate model for many biochemical reactions taking place between membrane components is a photochemical reaction in which both reactants reside in the membrane, one of them being created at a given moment by absorption of light. In principle, the kinetics of such model reactions is straightforward and may be followed in time-resolved experiments where a light pulse with a short duration, compared with the subsequent kinetics, triggers the reaction.[2] As usual, the kinetics can also be derived from the analysis of the time evolution of reactant and/or product concentration in continuous irradiation. In this approach many kinetic details are lost but there is the advantage of detecting the cumulative effect in reactant disappearance and product formation.

Due to the low molecular diffusion coefficients in the membrane, and also due to the two-dimensional constraints, the rate constant for a diffusion controlled reaction, k_{diff}, is strongly time-dependent, being more appropriately called rate *coefficient* and denoted by $k_{diff}(\zeta)$, where ζ represents the time scrolled after the excitation event. In an ideal time-resolved experiment all the excited reagent is created at $t = 0$ enabling a direct observation of $k_{diff}(\zeta)$, because ζ and t, the time of observation of the change in reagent concentration, are the same. In steady-state irradiation, because we are constantly creating new reagent and analyzing the time evolution of reagents and products in the much larger time scale of the irradiation process, only an average value of $k_{diff}(\zeta)$ can be obtained. So, the relevant question is how does this averaged rate constant relate to the molecular parameters, diffusion coefficient and collisional distance, for a given reactional geometry.

A steady-state irradiation is equivalent to a series of single identical and consecutive light pulses. At a given time ζ after each pulse, the fraction of excited molecules formed in this event that decay through the reaction pathway is $k_{diff}(\zeta)C/[k_{diff}(\zeta)C + 1/\tau_0]$, where τ_0 is the unquenched lifetime of the species and C the concentration of reactant considered constant in the ζ time scale. An average value of $k_{diff}(\zeta)$ for this light pulse, defined as the rate constant that would result in the same conversion, may be obtained from the integration in ζ of the above expression, weighted by the fraction of excited molecules still existing at ζ. However, as the irradiation proceeds this average

* Address correspondence to this author at Eurico Melo Instituto de Tecnologia Química e Biológica, Apartado 127, P-2781-901 Oeiras, Portugal. E-mail: eurico@itqb.unl.pt.

[†] Instituto de Tecnologia.

[‡] Instituto Superior Técnico.

10.1021/jp9918196 CCC: $18.00
Published on Web 11/13/1999

SCHEME 1

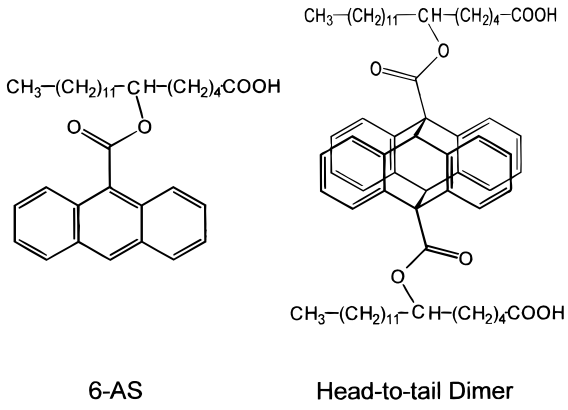

value changes due to the decrease in C, contrary to what happens in the case where k_{diff} is a constant. In fact $k_{diff}(\zeta)$ decrease with ζ, and, if in the beginning of the irradiation, high C, most of the reaction takes place shortly after excitation, therefore with a high rate coefficient; by the end of the irradiation, when C is very low, the quenched lifetime becomes large allowing many molecules to react with a lower rate coefficient. Hereafter $k_{diff}(C)$ will be used to represent this averaged diffusion rate coefficient, $k_{diff}(C) = \langle k_{diff}(\zeta)|C\rangle$.

From the comparison of the theoretical predictions with the experimental results of a steady-state irradiation it is, in principle, possible to recover $k_{diff}(\zeta)$ and the molecular parameters and the geometric constraints for diffusion used in its definition. The question of which is the more appropriate expression for $k_{diff}(\zeta)$ to be used in each case is of great practical importance, not only because correct molecular parameters concerning the diffusion and reaction need a correct description of the geometrical conditions but also because we must be aware that there are cases for which different models do not predict experimentally distinct results. In reactions that take place in nonviscous three-dimensional media the transient effects are negligible and the diffusion-controlled rate coefficient may be taken as constant. However, for 3D viscous media the time dependence of the diffusion-controlled rate coefficient may become important as predicted theoretically[3,4] and largely experimentally confirmed.[5] Unlike what happens in the three-dimensional case, in two-dimensions the rate coefficient of a diffusion-controlled reaction is continuously variable and tends to zero as the reaction proceeds.[6,7] This theoretical prediction has been experimentally verified for the pyrene excimer formation reaction.[2]

It is to note that, intrinsically, the phospholipid bilayer is a reaction media of reduced dimensionality and, if the reactant characteristics are such that it can only diffuse in the plane of the bilayer, the reaction takes place in purely 2D geometry. If the reactant can move across the bilayer (case of small and/or nonamphiphilic reactant molecules), the reactant diffusion may not be strictly described by the 2D law but it is certainly not described by the 3D law because this would require a random isotropic diffusion in 3 dimensions.

In this work we study the reaction between an excited and a ground-state 6-AS molecule to yield a head-to-tail photodimer by steady-state irradiation, taking into account the premises previously presented, Scheme 1.

Kinetics of Photodimerization

By analogy with what has been observed in homogeneous media for 12-AS,[8] the photodimerization of 6-AS in POPC bilayers, when irradiated with the 366 nm mercury line, may be represented by the general kinetic Scheme 2.

SCHEME 2

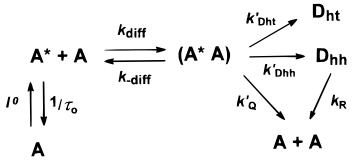

SCHEME 3

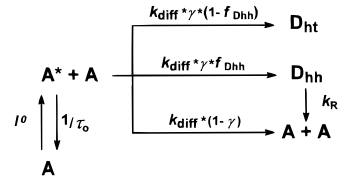

In this kinetic scheme we consider the formation of both isomers, the head-to-tail (ht) and the head-to-head (hh) dimers, and the thermal reversibility of the latter. This is done because, as we have previously shown, although thermally very unstable the D_{hh} of these 9-anthroate esters is formed.[8] In work previous to ours the head-to-head dimers of 9-anthroate derivatives escaped detection due to its short lifetime, of the order of some minutes, while for other 9 substituted anthracenes, e.g., 9-methylanthracene, it is of several hours.[9,10] Photochemically both dimers revert to the monomer,[11,12] but at our excitation wavelength the dimers do not absorb.[13]

If $k'_{D_{ht}} + k'_{D_{ht}} + k'_Q$ is much higher than the rate constant for the breakdown of the encounter complex by back diffusion, $k_{-\,diff}$, the quenching of the excited state is a diffusion controlled process. In this way there is no need to consider the encounter complex (A* A), for which case Scheme 2 is simplified as shown in Scheme 3.

This simplification is confirmed by the results obtained for benzyl 9-anthroate in benzene where the sum of the dimerization and self-quenching rate constant is higher than 10^{10} s^{-1},[14] while in our system the calculated values of $k_{-\,diff}$ vary from 6×10^7 to 1.4×10^8 s^{-1}.

According to Scheme 3 the kinetics of photodimerization of 6-AS in POPC bilayers can be modeled by the following set of differential equations:

$$\begin{aligned}
\frac{d[A^*]_l}{dt} &= -I_{abs} + \frac{1}{\tau_0}[A^*]_l - (1-2\gamma)k^{diff}([A]_l)[A]_l[A^*]_l \\
\frac{d[A^*]_l}{dt} &= I_{abs} - \frac{1}{\tau_0}[A^*]_l - k^{diff}([A]_l)[A]_l[A^*]_l \\
\frac{d[D_{ht}]_l}{dt} &= \gamma(1-f_{D_{hh}})k^{diff}([A]_l)[A]_l[A^*]_l \\
\frac{d[D_{hh}]_l}{dt} &= \gamma\, f_{D_{hh}}\, k^{diff}([A]_l)[A]_l[A^*]_l - k^R[D_{hh}]
\end{aligned} \tag{1}$$

where τ_0 is the unquenched fluorescence lifetime, $\gamma = (k'_{D_{ht}} + k'_{D_{hh}})/(k'_{D_{ht}} + k'_{D_{hh}} + k'_Q)$ the dimerization efficiency, $f_{D_{hh}} = k'_{D_{hh}}/(k'_{D_{hh}} + k'_{D_{ht}})$ the fraction of dimer formed as D_{hh}, k_R the rate constant for the thermal reversibility of D_{hh}, $k_{diff}([A]_l)$ the averaged diffusion rate coefficient and the subscript l means that the concentration is referred to the lipid pseudo-phase volume or area depending on the geometry considered for the calculation of k_{diff}. In the same way I_{abs} is the light absorbed by A in einstein s^{-1} dm^{-3} or einstein s^{-1} cm^{-2}.

To calculate $k_{diff}([A]_l)$ knowing the mutual diffusion coefficient (D_{eff}) we have to impose a model for the diffusion-controlled process, $k_{diff}(\zeta)$. In this work we compare the predictions of the diffusion model for 2D geometry, eq 2a, with those for 3D geometry when transient effects are taken into account, eq 2b, and when they are neglected, $k_{diff} = 4\pi R_c D_{eff} N'$.

$$k_{diff}(\zeta) = \frac{8 D_{eff} N_A}{\pi} \int_0^\infty \exp(-\alpha\beta^2) \frac{d\beta}{\beta[J_0^2(\beta) + Y_0^2(\beta)]} \qquad (2a)$$

$$\alpha = \frac{D_{eff}\zeta}{R_c^2}$$

$$k_{diff}(\zeta) = 4\pi R_c D_{eff} N' \left(1 + \frac{R_c}{\sqrt{\pi D_{eff}\zeta}}\right) \qquad (2b)$$

where D_{eff} is the mutual diffusion coefficient ($D_A + D_{A^*}$), $N' = N_A/1000$, $J_0(\beta)$ and $Y_0(\beta)$ are the zero-order Bessel functions of the first and second kind, respectively, and β is a dummy integration variable.

The average value of k_{diff} (ζ) is given by

$$k_{diff}([A]_l) = \langle k_{diff}(\zeta)|[A]_l\rangle = \int_0^\infty k_{diff}(\zeta)[A^*]_l(\zeta)d\zeta / \int_0^\infty [A^*]_l(\zeta)d\zeta \quad (3)$$

where the decay of the excited-state reactant is given by the usual eq 4.

$$[A^*]_l(\zeta) \propto \exp\left(-\frac{\zeta}{\tau_0} - \int_0^\zeta k_{diff}(u)[A^*]_l(\zeta)du\right) \qquad (4)$$

The integrals in eq 3 have an analytical solution for the diffusion in 3D,[5] Equation 5.

$$k_{diff}([A]_l) = \frac{1}{\tau_0[A]_l}\left\{\frac{1 + 4\pi R_c D_{eff} N' \tau_0 [A]_l}{1 - (\lambda/2)\sqrt{\pi}\exp(\lambda^2/4)\,\mathrm{erfc}(\lambda/2)} - 1\right\} \qquad (5)$$

$$\lambda = \frac{8\pi R_c^2 N' [A]_l \sqrt{\pi\tau_0 D_{eff}}}{\sqrt{1 + 4\pi R_c D_{eff} N' \tau_0 [A]_l}}$$

In Figure 1 panels a and b present the reaction kinetics in the ζ time scale for unquenched fluorescence lifetimes of 10 and 200 ns, respectively. The other parameters, the concentration of A, and D_{eff} are the same for all plots and correspond to a probe-to-lipid ratio of 1:50 and 5.0×10^{-8} cm^2 s^{-1} respectively. The two sets of curves in each plot are the rate of the diffusion-controlled process (probability that A* collides with A) and the normalized decay of the excited species. In each set the prediction for a 2D geometry is compared with that expected for 3D.

As a first observation, the quenching of a species with a 10 ns lifetime under those conditions is very small even for the high concentration used. In this case, the dependence of the averaged k_{diff} on $[A]_l$ is negligible, because the variation of k_{diff} results from the change of the quenched lifetime of A* due to the decrease of $[A]_l$ as explained previously. In case b, a very similar and significant quenching is predicted for both 2D and 3D systems but it is clearly wrong to neglect the time dependence of the diffusion rate constant.

In the second set of curves we represent the rate of the diffusion controlled process, $\upsilon(\zeta) = k_{diff}(\zeta)[A]_l[A^*]_l(\zeta)/[A^*]_l(0)$. Where, as previously, $[A]_l$ is the concentration in moles per unit surface or volume depending on the geometry being 2D or 3D. As a working hypothesis the volume of the lipid pseudophase is calculated considering that all the thickness of the bilayer is accessible to the reactive groups. The relative speed of reaction depends on the method used for calculation of the concentrations and will be discussed later.

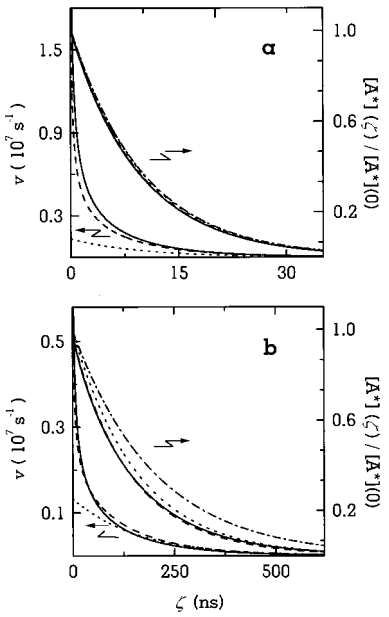

Figure 1. Rate of the diffusion controlled process (υ) as a function of time after excitation (ζ), $\upsilon(\zeta) = k_{diff}(\zeta)[A]_l[A^*]_l(\zeta)/[A^*]_l(0)$. For a 2D (—) and a 3D (- -) model for the lateral diffusion, also shown for 3D without transient effects (···). In the other set of curves is the normalized decay of A*, without quenching (- · -), and as the result of quenching due to the diffusion controlled process with the diffusion models: 2D (—), 3D (- -) and 3D without transient effects (···). Simulations for a POPC bilayer and also: $D_{eff} = 1.0 \times 10^{-7}$ cm^2 s^{-1}, reactant-to-lipid ratio of 1:50 and [lipid] $= 1 \times 10^{-3}$ M. In plot a $\tau_0 = 10$ ns, and in plot b $\tau_0 = 200$ ns.

The prediction with a time independent rate coefficient is again significantly different from that obtained with the complete rate laws. As expected the difference between the curves is smaller for the larger lifetime.

The fit of the model, eq 1, to the experimental results is obtained by adjusting only one parameter, γ, the other 5 being independently determined. The rate of excitation was obtained by measuring the light intensity and calculating the absorbed intensity taking into account the bandwidth and wavelength used in the experiment. The rate of unimolecular deactivation of the excited reactant was obtained from fluorescence lifetime measurements. The fraction of dimer formed as D_{hh} and its thermal reversibility rate constant were also previously known from a separate experiment. Finally, from the diffusion coefficient measured with FRAP, the diffusion rate constant is calculated using either the 2D or 3D diffusion model, eqs 2 and 3.

We also recover the constant that converts $[A^*]_l$ in the fluorescence intensity measured. This constant is the product of the radiative rate constant of the fluorescent probe and the equipment efficiency factor.

Materials and Methods

Materials. For all solutions sodium phosphate buffers 10^{-2} M, pH = 7, in Millipore Q water were used. All solvents are spectroscopic or HPLC grade from Merck or Riedel-de Haën. 6-AS and NBD-hexadecylamine are from Molecular Probes

(Eugene, OR) and POPC is from Avanti Polar Lipids (Birmingham, AL); all were used without further purification.

Steady-State Photodimerization. The kinetics of photodimerization was studied using a SPEX Fluorolog 212 with the lamp replaced by a 100 W Hg lamp in a PTI focusing housing. The irradiation wavelength was 366 nm. The molar absorption coefficient (ϵ) used for the calculation of I_{abs} in eq 1 was determined by calculating the overlap between the absorption spectra and the lamp plus monocromator profile, using $\epsilon_{364\ nm} = 6800\ M^{-1}\ cm^{-1}$. The intensity of the excitation beam was determined by potassium ferrioxalate actinometry. For each experiment the light intensity is corrected by comparison of the reference signal with the one obtained during the actinometry measurement. To obtain a lower intensity a neutral density filter was used.

In the photodimerization experiment, 0.5 cm^3 of a multi lamellar vesicle (MLV) suspension, was deaerated by bubbling argon, which at the same time promotes solution homogenization. The reaction was followed by the fluorescence intensity of the reactant in a right angle geometry.

Quantification of both 6-AS and POPC in each sample and analysis of irradiation products was performed by HPLC with diode array absorption detector (Merck-Hitachi), using an RP-18 column with methanol:acetonitrile:water (90:8:2) as the mobile phase and a column temperature of 40 °C.

Calculations. To calculate the concentration of reactant in the lipid pseudo-phase the dimensions of POPC in the bilayer are needed. In the absence of these values in the literature we have used those for DOPC[15] which should not be significantly different, being the area occupied by the phospholipid 0.6 nm^2, and the thickness of one monolayer 2.2 nm (measured from the coline group to the center of the bilayer). In the calculation of $k_{diff}(\zeta)$ we used the collisional distance, R_C, between two anthroate moieties obtained from the theory of Edward,[16] $R_C = 2R_{anthroate} = 0.7$ nm.

The time evolution of 6-AS and dimer concentrations were calculated by numerical integration of eq 1 using the Gear method for numerical solution of stiff differential equations.[17] The fit of eq 1 to the experimental data was done with the Simplex algorithm. All calculations were performed in a personal computer using FORTRAN routines.

Time-Resolved Fluorescence. Time-resolved fluorescence experiments were obtained by time-correlated single-photon counting with an experimental setup described elsewhere.[18] Using the 337 nm emission line of a conventional pulsed N_2 lamp for excitation.

FRAP. The diffusion coefficients were obtained by FRAP using an experimental setup described elsewhere,[19,20] with a uniform circular beam profile of radius of 3.1 or 4.5 μm (Zeiss Neofluar 10/0.30 or 6.3/0.20, respectively). The beam dimensions were calibrated considering the well-known diffusion coefficient of NBD-POPE in POPC bilayers at 25 °C.[21] The recovery was analyzed with the law for a circular beam profile.[22,23] The data acquisition and shutter control were made with an WorkMate board using the WorkBench PC for Windows Software (Strawberry Tree).

Head-to-Head Dimer Kinetics. The irradiation was performed with the 366 nm line of a 1000 W Hg lamp in a PTI focusing housing at a temperature of 20, 30, or 40 °C, during less than 5 min. For each temperature two experiments were made. The reversibility of D_{hh} was followed by the decrease in its concentration and/or by the concomitant increase in [6-AS]. The concentrations were obtained by HPLC with an RP-18 column and methanol with 0.5% of trifuoroacetic acid 0.6% in water as the mobile phase, at room temperature (20 ± 1 °C).

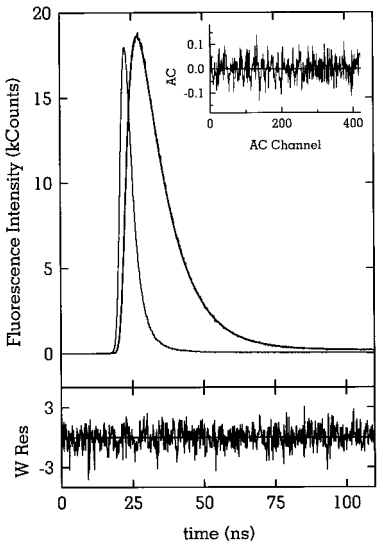

Figure 2. Lifetime decay of 6-AS in POPC (1:1000) at 25 °C, and best fit. Recovered parameters in Table 1.

TABLE 1: Unquenched Lifetime, τ_0, of 6-AS and Lateral Diffusion Coefficient, D, for NBD-Hexadecylamine in POPC Bilayers[a]

T (°C)	τ_0 (ns)	D (10^{-8} cm^2 s^{-1})
20	10.6 ± 0.2	4.2 ± 0.4
25	9.6 ± 0.2	5.0 ± 0.7
30	8.7 ± 0.2	6.5 ± 0.6
40	7.3 ± 0.2	8.6 ± 0.8
50	6.2 ± 0.2	12 ± 1

[a] The presented unquenched lifetimes were obtained for a concentration of 1:200 (at least two experiments for each temperature) and were nearly independent of the probe concentration in the range from 1:1000 to 1:50 (results not shown). The lateral diffusion coefficient were obtained by FRAP for a 1:2000 probe-to-lipid ratio (at least five experiments for each temperature, three different samples).

Results and Discussion

Fluorescence Lifetime Measurements. The fluorescence decay of 6-AS in POPC bilayers follows the usual pattern found for the 9-anthroate esters.[18,24] When excited, the 9-anthroates became planar and the resonance extends to the carboxylate group, and as a consequence of this the absorption spectra, anthracene-like, is quite different from the fluorescence emission which is unstructured and strongly Stokes shifted. The speed at which the carboxylate group rotates to give the relaxed excited state is solvent dependent. This rotation is revealed in the time dependence of the shape of the emission spectra with a larger contribution at short times of an anthracenoid emission which convert in the longer lived, longer wavelength emitting, relaxed form. At the isosbestic wavelength, where the component arising from the appearance of the relaxed state cancels the one originated in the nonrelaxed form, the decay is apparently single exponential with the relaxed form lifetime.[18,24] The measurements were made at or close to this wavelength, Figure 2.

Given the short lifetime of 6-AS no significant decrease, which would result from quenching due to the collision of two 6-AS molecules, is observed in a concentration range from 1:1000 to 1:50 probe-to-lipid ratio. In Table 1 the unquenched lifetimes for 6-AS at several temperatures are presented.

Head-to-Head Dimer Kinetics. The fraction of dimer formed in the head-to-head configuration, $f_{D_{hh}}$, and the reversibility rate

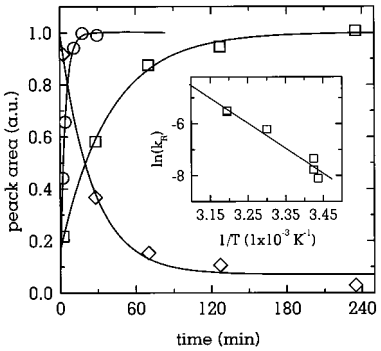

Figure 3. Thermal reversibility of D_{hh}, as determined by HPLC. Peak area of 6-AS (□), and D_{hh} (◇) at 20 °C, and of 6-AS at 40 °C (O). Insert: Arrenhius plot of k_R, $E_a = 80$ kJ mol^{-1}, k_R (T = ∞) = 1×10^{11} s^{-1}.

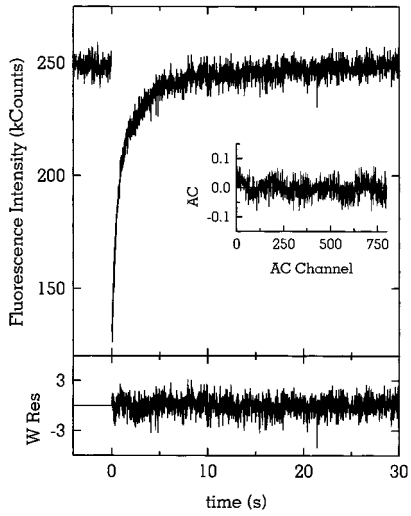

Figure 4. FRAP experiment for NBD-hexadecylamine in POPC multibilayers at 25 °C, the probe-to-lipid ratio is 1:2000. Recovered parameters in Table 1.

constant, k_R, were obtained by irradiation of a solution of 6-AS in POPC with a reactant-to-lipid ratio of 1:20, Figure 3.

At 20 °C the reversibility of D_{hh} was followed by the increase in the concentration of 6-AS and a concomitant decrease in the D_{hh} concentration, both leading to the same result, $k_R = 5(\pm 2) \times 10^{-4}$ s^{-1}. At 30 and 40 °C, the reversibility is much faster and only the increase in the 6-AS concentration was followed, giving, respectively, $k_R = 2.0(\pm 0.5) \times 10^{-3}$ and 4 (± 1) $\times 10^{-3}$ s^{-1}. For all temperatures $f_{D_{hh}} = 0.25 \pm 0.05$.

Reactant Diffusion Coefficients. To independently evaluate the diffusion coefficient of the anthroate derivatized lipid we have measured the long-range diffusion coefficient of the model compound NBD-hexadecylamine in the temperature range 20−50 °C, Figure 4 and Table 1.

The diffusion coefficient obtained at 25 °C is $5.0(\pm 0.7) \times 10^{-8}$ cm^2 s^{-1}and the activation energy for diffusion is 30 ± 2 kJ mol^{-1}. Those values of the diffusion coefficient and activation energy were used for the case of 6-AS molecule in POPC bilayers. Given the difference between the two molecules this procedure deserves further explanation.

It is known from literature that the lateral diffusion coefficient of phospholipid probes with the NBD group attached to the ethanolamine headgroup in POPC bilayers does not present a significant dependence on the probe chain length. For example, the diffusion coefficient for *N*-(NBD)1-palmitoyl-2-oleoyl-*sn*-glycero-3-phosphoethanolamine at 25 °C is $4.2(\pm 0.4) \times 10^{-8}$ cm^2 s^{-1}, similar to what is obtained with the probe attached to 1,2-C_{12}, 1,2-C_{16}, and 1,2-C_{18}.[21] In egg phosphatidylcholine bilayers at the same temperature the diffusion coefficient for *N*-(NBD)phosphatidylethanolamine, *N*-(NBD)lysophosphatidylethanolamine and 1-acyl-2-(NBD)caproyl-phosphatidylcholine are $6.3(\pm 0.4) \times 10^{-8}$, $7.1(\pm 0.6) \times 10^{-8}$, and $5.9(\pm 0.2) \times 10^{-8}$ cm^2 s^{-1}, respectively.[25] We conclude that the position of the NBD probe in the head or in the tail of the same phospholipid does not introduce a significant change in the diffusion coefficient at this temperature, in the same way the diffusion of a single hydrocarbon tail does not differ significantly from the diffusion of the double tail molecule. Therefore we do not expect any significant difference between the diffusion coefficient of 6-AS and NBD-hexadecylamine.

In what concerns the activation energy for diffusion the results obtained for the NBD derivatives discussed above lead to a similar conclusion ($E_a = 30 \pm 2$ kJ mol^{-1} for NBD-hexadecylamine and also ca. 30 kJ mol^{-1} for the other compounds.[21,25,26]

A further concern is the possibility that C_{16}−NBD may exchange between the bilayer and water originating an apparent increase of the diffusion coefficient. This possibility was discarded by testing, using the change in fluorescence anisotropy, the exchange of the probe between LUVs of DMPC and DSPC. The variation in fluorescence anisotropy was non measurable in a time scale of several minutes leading us to the conclusion that no exchange takes place in this time scale (results not shown). The solubility of *n*-AS in aqueous solutions has also been reported as negligible.[8]

In this way we consider that C_{16}-NBD is an appropriate probe to mimic the lateral diffusion of 6-AS in phospholipid bilayers.

Steady-State Photodimerization. The photodimerization efficiency, γ, was obtained for four different 6-AS:POPC ratios: 1:1000, 1:500, 1:100, and 1:50. Two different irradiation light intensities have also been used in the experiments at 25 °C. In principle there should be no reason for variation of γ with the reactant concentration, the constancy of γ being a test of the kinetic model used, Scheme 3, eqs 1−3.

In Table 2 we present the recovered value of γ for the three diffusion models considered. As predicted in the kinetics section, $k_{diff}([A]_l)$ does not show a significant dependence on $[A]_l$ (or time of irradiation) for a concentration up to 1:50 reactant-to-lipid ratio due to the short lifetime of the excited species. The value used for $k_{diff}([A]_l)$ in eq 1 was the same for all reactant concentrations at each temperature and is also presented in Table 2.

The quality of the fit is always quite good for all models. In Figure 5 we present the best fit using the 2D model for the cases: 25 °C, 1:1000 and 1:500, and 40 °C, 1:100 and 1:50. The value of χ^2 is always larger than one due to the residuals being weighted only by the standard deviation in the fluorescence detection, not counting for the noise created by the bubbling used for mixing and deaeration. Since the weighted residuals are always good, we cannot judge the model used from the quality of the fit; but this can be done from an analysis of the parameters retrieved with each model.

The value obtained for the dimerization efficiency from the two-dimensional geometry, $\gamma \approx 0.07$, is similar to that obtained for 12-AS in micelles of $C_{12}E_{10}$, $\gamma = 0.1$.[8] Since there is no reason to expect a dependence of the dimerization efficiency with the surrounding medium, the similarity of the two values indicates that the 2D model is correctly predicting the efficiency. Moreover γ is independent of the temperature, as it should be. We did not expect also any dependence of γ on the reactant concentration and light intensity. However, we observe that the

TABLE 2: Photodimerization Efficiency, γ, Recovered from the Best Fit of Eq 1 to the Experimental Results[a]

		3D steady		3D transient		2D	
T (°C)	6-AS:POPC	k_{diff} (M^{-1} s^{-1})	γ	k_{diff}[b] (M^{-1} s^{-1})	γ	k_{diff}[b] (cm^2 s^{-1} mol^{-1})	γ
20	1:500	4.4×10^7	0.27 ± 0.02	1.5×10^8	0.08 ± 0.01	8.9×10^{17}	0.06 ± 0.01
25	1:1000	5.3×10^7	0.34 ± 0.04	1.7×10^8	0.11 ± 0.02	1.0×10^{18}	0.08 ± 0.02
	c		0.40 ± 0.05		0.13 ± 0.02		0.10 ± 0.02
	1:500		0.28 ± 0.04		0.085 ± 0.01		0.07 ± 0.01
	c		0.32 ± 0.04		0.10 ± 0.01		0.08 ± 0.01
	1:100		0.25 ± 0.02		0.08 ± 0.01		0.065 ± 0.01
	1:50		0.20 ± 0.02		0.065 ± 0.01		0.055 ± 0.01
30	1:500	6.9×10^7	0.25 ± 0.02	2.1×10^8	0.08 ± 0.01	1.2×10^{18}	0.065 ± 0.01
40	1:1000	9.1×10^7	0.30 ± 0.05	2.7×10^8	0.12 ± 0.02	1.6×10^{18}	0.10 ± 0.02
	1:500		0.29 ± 0.04		0.10 ± 0.01		0.08 ± 0.01
	1:100		0.27 ± 0.02		0.10 ± 0.01		0.075 ± 0.01
	1:50		0.22 ± 0.02		0.08 ± 0.01		0.06 ± 0.01
50	1:500	1.3×10^8	0.28 ± 0.03	3.6×10^8	0.10 ± 0.01	2.0×10^{18}	0.08 ± 0.01

[a] The rate constants I^0, τ_0, and k_{diff}, were fixed; $f_{D_{hh}}$ and k_R were left free to change inside the interval $\pm 25\%$ of the experimentally obtained mean value whenever this gave a significant improvement in the quality of the fit. For each reactant concentration and temperature more than one experiment were made but all with the same sample preparation. [b] For the models, 2D and 3D with transient effects, the dependence of k_{diff} with the reactant concentration is very slight, it changes less than 1% for a concentration up to 1:50. The values presented were used to find the best fit for all concentrations. [c] In these experiments the light intensity was $I^0 = 1.8 \times 10^{-5}$ einstein dm^{-3} s^{-1}; for all other experiments it was $(7.5 \pm 0.3) \times 10^{-5}$ einstein dm^{-3} s^{-1}.

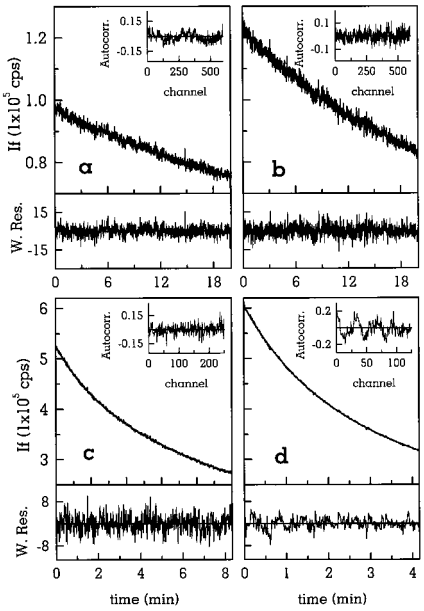

Figure 5. Steady-state dimerization of 6-AS in POPC bilayers and best fit with the model for a 2D geometry. A, 1:1000, 25 °C; B, 1:500, 25 °C; C, 1:100, 40 °C; D, 1:50, 40 °C. Recovered parameters in Table 2.

increase of either reactant A or A* leads to a small decrease in the dimerization efficiency which can only be explained by the existence of a residual side reaction, either with oxygen or with lipid impurities.

For the analysis with the 3D diffusion model we need to know the thickness of the bilayer accessible to the reactant in order to calculate the volume of the lipid pseudo-phase, and consequently the reactant concentration. In the kinetics section, as a working hypothesis, we have considered that all the thickness of one bilayer leaflet is accessible to the reactive groups. The same approach was used to fit the results and obtain the dimerization efficiency presented in Table 2. The value, $\gamma \approx 0.09$, does not differ from the one obtained using the 2D model, but the physical meaning of this approach is questionable. In fact, it is well established that the chromophore of the *n*-AS molecule when included in the phospholipid bilayer is at a given, well defined, mean position depending on the carbon of the fatty acid chain at which it is attached.[27,28] If, on the contrary, we consider only the region where the anthroate resides, the available lipid pseudo-phase volume is about $^1/_3$ of the total lipid volume (reactant diameter/thickness of the monolayer) and, the dimerization efficiency, $\gamma \approx 0.03$, is much smaller than expected. A similar value has been obtained for 12-AS in CTAC micelles but in this case the reaction is inhibited due to the interaction with the positively charged surfactant.[8]

The agreement of γ with the expected value in the 3D analyses obviously depends on the thickness of the bilayer because the calculated concentration, but not the kinetics, depend on it. Unfortunately the thickness of all fluid phospholipid bilayers do not differ by more than 20% and several other factors can affect the photodimerization efficiency more than this. Therefore this simple test cannot be done.

The applicability of a 3D diffusion model to a lipid bilayer raises several questions. The 3D approach only has meaning if we consider that the reactants diffuse during the lifetime of the species in any random direction. Given that the reaction proceeds in fact in a 2D geometry the expressions for diffusion in 3D can be used taking into account the geometric difference in the flow of the diffusing species such that in both geometries the flow is the same. For this to be verified the diffusion coefficient to be used in the 3D formalism, D'_{eff}, must relate with D_{eff} through the expression, $D'_{eff} = {}^2/_3 D_{eff}$. This correction will increase slightly the dimerization efficiency obtained, but all the above interpretations, based on the value of γ, are unchanged. However it must be kept in mind that if we were analyzing a true 3D reaction in an isotropic medium the diffusion coefficient obtained from FRAP should be used without correction, because FRAP measures the mean displacement of molecules in two dimensions, $\langle r \rangle$, related to the diffusion coefficient by $\langle r \rangle = \sqrt{4Dt}$, regardless of the existence of a third component for diffusion. In conclusion, whatever the approach, the use of a 3D model in this case is devoid of physical meaning, not because of the parameters obtained but because the model itself does not describe the physical system.

When in the 3D model we neglect the transient effects, $\gamma \approx 0.3$ is obtained, which is a very large value for this reaction. This dimerization efficiency is larger than the higher value found for 9-anthroate derivatives: for ethyl 9-anthroate in benzene γ

$= 0.2$,[29] which is reduced when ethyl is substituted by bulkier groups; $\gamma = 0.06$ for benzyl 9-anthroate in benzene;[14] and $\gamma = 0.1$ for 12-AS in $C_{12}E_{10}$ micelles.[8] This happens because, as we have already shown, for the high viscosity of a phospholipid bilayer the time dependence of the diffusion rate constant is significant during the first nanoseconds, Figure 1a, and, even in the case of a legitimate 3D system with these high viscosities, not considering the transient effects would be an error.

Conclusions

We have presented a model to describe steady-state diffusion controlled reactions involving an excited state reactant. The model, including the time dependence of the diffusion controlled rate constant, has been successfully applied to the photodimerization of 6-AS in POPC bilayers. It is shown that when the transient effects are neglected an overevaluated reaction efficiency is obtained.

Although the 3D model for diffusion, including the transient effects, fits the experimental data and gives an acceptable kinetic parameter, we consider that it does not describe the photodimerization of 6-AS in POPC bilayers because the basic assumptions for the 3D diffusion model are not acceptable (homogeneous distribution of concentrations and isotropic reaction media in three dimensions).

In conclusion we stress the need to use a 2D specific model in the analysis of diffusion controlled reactions whenever, as in our case, the collision takes place in a 2D geometry.

Acknowledgment. The research described herein was supported in part by the project PRAXIS/PCNA/C/BIA/168/96. We gratefully acknowledge the help of Dr. W. L. C. Vaz with the FRAP measurements and interpretation. M.J.M. thanks the Universidade do Algarve for a leave of absence that allowed the conclusion of this work.

References and Notes

(1) Melo, E. C. C.; Lourtie, I. M. G.; Sankaram, M. B.; Thompson, T. E.; Vaz, W. L. C. *Biophys. J.* **1992**, *63*, 1506.

(2) Martins, J.; Vaz, W. L. C.; Melo, E. *J. Phys. Chem.* **1996**, *100*, 1889.

(3) von Smoluchowski, M. *Phys. Z.* **1916**, *17*, 585.

(4) Sveshnikoff, B. *Acta Physicochim. URSS* **1935**, *3*, 257.

(5) Nemzek T. L., Ware W. R. *J. Chem. Phys.* **1975**, *62*, 477.

(6) Emeis C. A., Fehder P. L. *J. Am. Chem. Soc.* **1970**, *92*, 2247.

(7) Razi Naqvi, K. *Chem. Phys. Lett.* **1974**, *28*, 280.

(8) Moreno, M. J.; Lourtie, I. M. G.; Melo, E. *J. Phys. Chem.* **1996**, *100*, 18192.

(9) Cowan, D. O.; Schmiegel, W. W. *J. Am. Chem. Soc.* **1972**, *94*, 6779.

(10) Wolff, T.; Muller, N.; Von Bunau, G. *J. Photochem.* **1983**, *22*, 61.

(11) Robertson, W. W.; Music, J. F.; Matsen, F. A. *J. Am. Soc.* **1950**, *72*, 5260.

(12) Yamamoto, S.-A.; Grellmann, K.-H.; Weller, A. *Chem. Phys. Lett.* **1980**, *70*, 241.

(13) Yang, N. C.; Shold, D. M.; Kim, B. *J. Am. Soc.* **1976**, *98*, 6587.

(14) Costa, S. M. B.; Melo, E. *J. Chem. Soc., Faraday Trans. 2* **1980**, *76*, 1.

(15) Wiener, M. C.; White, S. H. *Biophys. J.* **1992**, *61*, 434.

(16) Edward, J. T. *J. Chem. Educ.* **1970**, *47*, 261.

(17) Gear, C. W. *Numerical Initial Value Problems in Ordinary Differential Equations*; Prentice-Hall: Englewood Cliffs, NJ, 1971.

(18) Maçanita, A. L.; Costa, F. P.; Costa, S. M. B.; Melo, E. C.; Santos, H. *J. Phys. Chem.* **1989**, *93*, 336.

(19) Criado, M.; Vaz, W. L. C.; Barrantes, F. J.; Jovin, T. M. *Biochemistry* **1982**, *21*, 5750.

(20) Jovin, T. M.; Vaz, W. L. C. *Methods Enzymol.* **1989**, *172*, 471.

(21) Vaz, W. L. C.; Clegg, R. M.; Hallmann, D. *Biochemistry* **1985**, *24*, 781.

(22) Axelrod, D.; Koppel, D. E.; Schlessinger, J.; Elson, E.; Webb, W. W. *Biophys. J.* **1976**, *16*, 1055.

(23) Soumpasis, D. M. *Biophys. J.* **1983**, *41*, 95.

(24) Melo, E.; Costa, S. M. B.; Maçanita, A. L.; Santos, H. *J. Colloid Interface Sci.* **1991**, *141*, 439.

(25) Derzko, Z.; Jacobson, K. *Biochemistry* **1980**, *19*, 6050.

(26) Vaz, W. L. C.; Derzko, Z. I.; Jacobson, K. A. In *Membrane Reconstitution*; Poste, G., Nicolson, G. L., Ed.; Elsevier Biomedical Press: Amsterdam, The Netherlands, 1982; Chapter 3.

(27) Thulborn, K. R.; Sawyer, W. H. *Biochim. Biophys. Acta* **1978**, *511*, 125.

(28) Villalaín, J.; Prieto, M. *Chem. Phys. Lipids* **1991**, *59*, 9.

(29) Shon, R. S.-L.; Cowan, D. O.; Schmiegel, W. W. *J. Phys. Chem.* **1975**, *79*, 2087.